

The Compressible Ising Spin Glass: Simulation Results

Adam H. Marshall

The James Franck Institute and Department of Physics, University of Chicago, Chicago, Illinois 60637

(Dated: May 25, 2019)

This paper reports numerical studies of a compressible version of the Ising spin glass in two dimensions. Compressibility is introduced by adding a term that couples the spin-spin interactions and local lattice deformations to the standard Edwards-Anderson model. The relative strength of this coupling is controlled by a single dimensionless parameter, μ . The timescale associated with the dynamics of the system grows exponentially as μ is increased, and the energy of the compressible system is shifted downward by an amount proportional to μ times the square of the uncoupled energy. This result leads to the formulation of a simplified model that depends solely on spin variables; analysis and numerical simulations of the simplified model predict a critical value of the coupling strength above which the spin-glass transition cannot exist at any temperature.

PACS numbers: 75.10.Nr, 75.40.Mg, 05.50.+q

I. INTRODUCTION

Much theoretical study has been made of the nature of the spin-glass transition. It is now generally accepted that the three-dimensional spin glass undergoes a second-order phase transition at finite temperature,^{1,2,3,4,5,6,7} and the bulk of the evidence in two dimensions suggests that there is a zero-temperature phase transition,^{5,8,9,10,11,12} although recent work suggests that the lower critical dimension for some spin-glass models is greater than two.¹³ The continued controversy hints at the delicate and subtle nature of the spin-glass transition and suggests that modifications to the underlying model, even small ones, could have dramatic effects on the system.

Compressibility has already been shown to have a strong effect on a variety of spin systems. The inclusion of compressibility in the Ising ferromagnet modifies the standard second-order transition to a first-order transition that occurs at the Curie temperature.^{14,15} The (fully frustrated) 2-D triangular Ising anti-ferromagnet does not undergo a phase transition; however, when compressibility is added to the model, the characteristic frustration is relieved, and the system develops a first-order transition to a “striped” phase at low temperatures.^{16,17,18} Other frustrated spin systems are known to have their frustration relieved by the presence of magnetoelastic couplings,^{19,20} and polaron effects alter the nature of magnetic transitions in frustrated physical systems such as manganites.^{21,22,23}

With the possibility of relieving frustration, the addition of compressibility to spin-glass models could dramatically alter the nature of the spin-glass phase and/or the transition thereto. Furthermore, the fact that all physical systems must possess some (albeit small) spin-lattice coupling provides a physical motivation for such studies.

A previous paper introduced a particular model for the compressible spin glass with a linear coupling between the spin-spin interactions and the distances between neighboring particles.²⁵ The work described there involved simulations of the compressible spin glass per-

formed on two-dimensional systems in which the volume was held fixed. Results of the direct simulations suggest a simplified model, qualitatively equivalent to the first, that depends only upon spin degrees of freedom. The presence of compressibility alters the preferred spin configurations of the system, so that the transition to a low-temperature spin-glass phase is impossible above a critical value of the coupling. The current paper expands on that previous work as well as provides details of the analysis. Presented here are results showing the exponential slowing down of the time to reach equilibrium as the coupling increases, additional quantitative motivation for the simplified model, and a functional form for the entropy of the spin glass, from which thermodynamic quantities are predicted. Finally, a phase diagram illustrates an approximate boundary separating critical behavior from the region where the spin-glass transition cannot exist.

The structure of this paper is as follows: Section II describes the Hamiltonian of the compressible spin glass and defines the important tuning parameters. The details of the computer simulations are discussed in Sec. III, and the results of the simulations are presented in Sec. IV. A simplified model is introduced in Sec. V, along with results of numeric simulations and analytic investigations performed on the simplified model. Section VI contains the primary conclusions and some additional points of discussion.

II. THE MODEL

The Hamiltonian for the compressible Ising spin glass is²⁵

$$\mathcal{H} = - \sum_{\langle i,j \rangle} J_{ij} S_i S_j + \alpha \sum_{\langle i,j \rangle} J_{ij} S_i S_j (r_{ij} - r_0) + U_{\text{lattice}}. \quad (1)$$

The first term is the standard Edwards-Anderson spin-glass Hamiltonian,²⁶ with the sum performed over pairs of nearest neighbors. The spins S_i are dynamic variables

which may take the values $+1$ or -1 . The interactions J_{ij} are chosen randomly from $\{\pm J\}$ with equal probability and are then held fixed; this collection of interactions represents a single realization of the quenched disorder central to the nature of the spin glass.

The coupling between the spin interactions and the lattice distortions is contained within the second term of Eq. (1), where the coupling is considered to linear order with proportionality constant α . This constant multiplies the change in bond length: r_{ij} represents the Euclidean distance between particles i and j , and r_0 is the natural spacing of nearest neighbors on the lattice. This term allows the system to lower the total energy by displacing the particles from their regular lattice positions. Spins with satisfied interactions (i.e., those with $J_{ij}S_iS_j = +1$) will tend to move closer together in order to strengthen the effect; similarly, unsatisfied bonds will tend to lengthen as the particles move farther apart to diminish the negative effect of their interaction on the total energy. The inability of all of the bonds in the system to distort simultaneously in the ideal fashion is the mechanism by which the degeneracy of configurations with equal spin-spin energy is broken.

The final term, U_{lattice} , stabilizes the lattice by providing a restoring force to counteract the displacements generated by the spin-lattice interactions. The stabilization is obtained by connecting harmonic springs between nearest neighbors and between next-nearest neighbors (along the diagonals of the square lattice). Each spring has as its unstretched length the natural spacing of the vertices, so that U_{lattice} is zero in the absence of spin-lattice coupling when the particles are not displaced.

Two important parameters can be formed. The first arises due to force balance between the last two terms in Eq. (1):

$$\bar{\delta} \equiv \frac{J\alpha}{k}, \quad (2)$$

This has dimensions of length and represents the scale of the typical displacements of the particles from their uncoupled locations on the square lattice. The second parameter is

$$\mu \equiv \frac{J\alpha^2}{k}, \quad (3)$$

which is dimensionless; it represents the strength of the spin-lattice coupling, relative to the spin-spin interaction. When $\mu = 0$, there is no spin-lattice coupling, lattice distortions are not energetically favorable, and the model reduces to the standard Edwards-Anderson spin glass. The interaction strength J serves merely to set the energy scale for the model. In this work, J is set to unity, while α and k are chosen so that $\bar{\delta}$ and μ take the desired values.

III. SIMULATION DETAILS

All simulations were run on square lattices of linear dimension L with periodic boundary conditions in two

dimensions; the size of the system was held constant in each direction, fixing the total volume. The control parameters were adjusted so that $\bar{\delta}$ was set at ten percent of the natural lattice spacing while μ was varied over the range $0 \leq \mu \leq 5$. Since the information regarding relative energy scales is contained within μ , the specific value of $\bar{\delta}$ does not affect the qualitative nature of the results, so long as the displacements are small enough to maintain the topology of the lattice. As discussed below, however, small nonlinearities do depend on the extent of the lattice distortions.

For all values of the control parameters, 100 different bond configurations (i.e., realizations of the quenched disorder) were simulated. Calculated quantities were then averaged over the various runs.

Two different methods of simulation were used to study the compressible spin glass. For the first method, suitable for studying the dynamics of the model, states were generated via single-spinflip Monte Carlo steps, with transition probabilities dependent upon the difference in energy between the two spin states. These energies employed the full Hamiltonian of Eq. (1), including the components that depend on the particle positions. For purposes of determining transition probabilities, the spins were considered to flip in place, i.e., without any particle motion. The lattice was then relaxed for the new spin configuration. The full simulation algorithm is as follows: The system is started in a random spin configuration with the particles located at the positions which minimize the total energy. From a given spin configuration, a particle is chosen at random. This particle is given a chance to flip, in place, from the state with energy E_1 to the state with energy E_2 . If $E_2 < E_1$ the spin is flipped; otherwise the spin flips with probability $\exp[-(E_2 - E_1)/T]$. After L^2 randomly chosen particles have been considered (i.e., one Monte Carlo step), the lattice is relaxed to the minimum of the potential energy for the new spin configuration using conjugate-gradient minimization. System properties are recorded for analysis, and this process is then repeated.

In order to ensure proper equilibration, I follow the algorithm prescribed by Bhatt and Young:^{1,5} The spin-glass susceptibility

$$\chi_{\text{sg}} = \frac{1}{L^2} \sum_{i,j} \langle S_i S_j \rangle^2,$$

where $\langle \cdot \rangle$ indicates a thermal (time) average, is calculated by two different methods, each as a function of equilibration time t_{equil} . One method uses the overlap between states of the same system at two different times during the run, while the other uses the overlap between states of two randomly initialized, independently run replicas of the same bond realization. These two computation methods produce the same value of χ_{sg} as $t_{\text{equil}} \rightarrow \infty$, but the “two-times” method approaches the asymptotic value from above, while the “two-replicas” method approaches from below. When the two values are within statistical error of one another, the system is equilibrated.

The simulations are typically run for several multiples of the equilibration time in order to acquire data from uncorrelated portions of the time evolution.

Another method of simulation, suitable for studying static properties such as the energy, involves substituting a collection of pre-generated spin states into the compressible spin-glass Hamiltonian and relaxing each to the minimum of its total energy with respect to the particle positions. Typically, the spin states are generated by single-spinflip Monte Carlo simulations using the standard (incompressible) spin-glass Hamiltonian, which takes much less time than simulations of the full Hamiltonian as described above. In this manner, “typical” states may be analyzed to observe the effect of the compressible terms on quantities of interest; however, these states will not occur with frequency given by the correct Boltzmann weight, so care must be taken not to draw conclusions that would rely on such an assumption. For the smallest system sizes ($L = 3, 4$, and 5), it was possible to enumerate all 2^{L^2} possible spin states for a given bond configuration.

For all methods of generating spin states, the lattice was relaxed to its minimum using the conjugate-gradient minimization technique.²⁷ Since the distortions of the lattice are kept small by the value of $\bar{\delta}$, the potential-energy landscape is close to quadratic, and the minimum can typically be located to reasonable numerical tolerance within a few conjugate gradient steps. Nevertheless, because of the computation involved in calculating the lattice energy, this portion of the simulation takes approximately two orders of magnitude more time than the Monte Carlo spinflips.

IV. RESULTS

Simulations of the two-dimensional, constant-volume compressible Ising spin glass were performed for system sizes ranging from $L = 3$ to 40 using the techniques described above. Data from these simulations are presented and analyzed below.

A. Dynamics

The time required for the system to reach thermal equilibrium is an easily accessible measure of the timescale for the system dynamics. For each value of μ , a different equilibration time is required, and Fig. 1 shows the dependence of the equilibration time, t_{equil} , on μ for the $L = 10$ systems at a relatively high temperature, $T = 2.0$. As the fit line on the semilog plot demonstrates, the growth of the equilibration time, in Monte Carlo steps (MCS), is exponential in μ ; the slope of the exponential fit is 1.8 MCS^{-1} . The rapid growth of the equilibration time as the coupling is increased can be viewed as a growth of energy barriers between states that

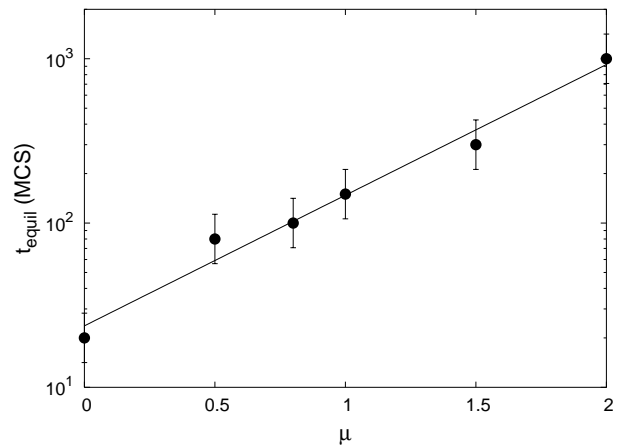


FIG. 1: The time to reach equilibrium, t_{equil} , grows exponentially as μ increases. The data here are from 100 $L = 10$ systems at $T = 2.0$, and the slope of the exponential fit line is 1.8 MCS^{-1} . The dramatic increase of simulation time makes straightforward simulation of the dynamics difficult for large values of the coupling.

were previously similar in energy. The movement of particles “locks in” the current spin configuration, increasing the timescale for single-spinflip transitions.

The growth of the equilibration time as a function of the coupling is in addition to the usual dramatic growth of dynamic timescales as the temperature is lowered (see, for example, Fig. 3 of Ref. 3). Since the number of simulation steps required increases exponentially with μ and the computation time per step increases in a manner proportional to the number of spins, direct simulations of the system dynamics at temperatures approaching the transition become prohibitive for large values of the coupling.

B. Energy Analysis

In analyzing the results of the simulations, the various components of the total energy may be computed independently for a given spin configuration. Of particular interest is the first term in Eq. (1). This component represents the contribution due solely to spin-spin interactions and is denoted E_0 . It is equivalent to the energy of that spin configuration on an undistorted lattice in the absence of any spin-lattice coupling.

As shown in Fig. 1 of Ref. 25, the effect of the coupling is to shift the states of the system downward in energy. When $\mu = 0$, the energy levels are δ -functions separated by constant gaps of $4J$, the smallest energy difference between states of the incompressible $\pm J$ model. As μ is increased from zero, each energy level (identified by E_0) shifts downward in energy and broadens into a Gaussian-shaped band.

For all of the states with a given value of E_0 , the distribution of energies is characterized by two values: the average shift in energy, $\Delta E(E_0, \mu) \equiv \langle E(E_0, \mu) \rangle - E_0$,

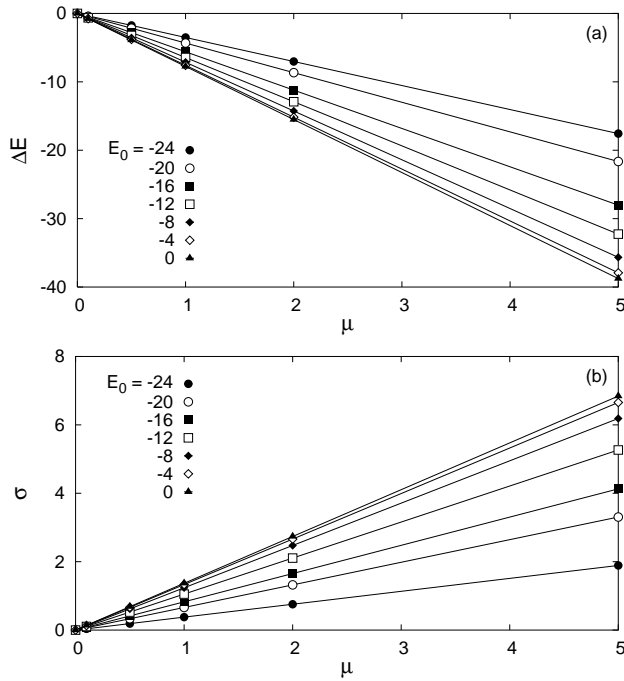


FIG. 2: The effect of the coupling on the energy for a single fully enumerated $L = 4$ system. (a) The average shift in energy, ΔE , is plotted as a function of the coupling μ . For each band of states, from $E_0 = -24$ (the ground-state energy for this particular system) to $E_0 = 0$, the energy shifts by an amount proportional to the coupling. (b) The width of each band, σ , is also proportional to μ .

and the width $\sigma(E_0)$ as given by the standard deviation of the distribution. Both ΔE and σ are linearly proportional to μ , as shown in Fig. 2. The data in that figure were obtained from a single $L = 4$ system using complete enumeration of all spin configurations; each line represents the data for a value of E_0 ranging from the ground-state energy for this specific system, $E_0 = -24$, to $E_0 = 0$, where there are equal numbers of satisfied and unsatisfied bonds.

The proportional dependences of both the energy shift and the width on μ are due to the fact that each spin state individually shifts by an amount exactly proportional to the coupling. When minimizing the potential energy of the lattice for a given spin configuration, the positions of the particles are determined by the value of $\bar{\delta}$; the value of μ then multiplies the result to determine the total energy in the distortions. Due to this fact, it is possible to characterize changes to the energy of the system at any convenient value of μ and then scale the obtained quantities by the coupling.

The lines shown in Fig. 2 have different slopes, indicating that the various bands shift and broaden at different rates as μ increases. The states with higher E_0 move downward in energy more rapidly than lower- E_0 states. Data for the shift in average energy from the uncoupled value, scaled by μ , are plotted as a function of original

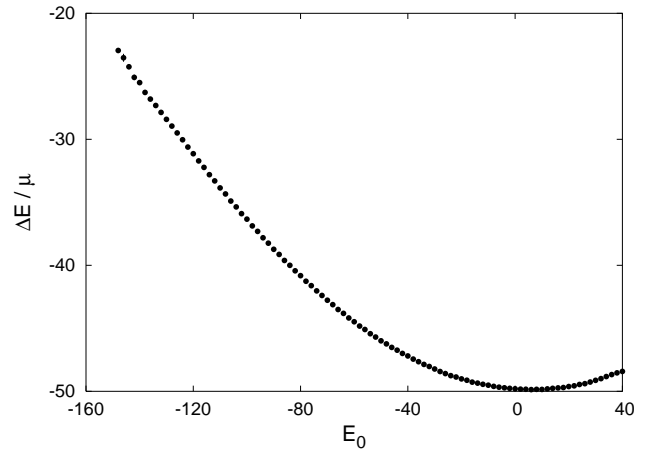


FIG. 3: Dependence of the energy shift on the spin-spin energy E_0 . These data are averaged over 100 $L = 10$ systems run at a variety of temperatures. The parabolic shape of this curve results from the fact that configurations with roughly equal numbers of short (satisfied) and long (unsatisfied) bonds can distort more effectively than those with many bonds of the same length.

energy level, E_0 , in Fig. 3; 100 systems with $L = 10$ and $\mu = 0.1$ were run at a sequence of temperatures and averaged to produce this plot. In practice, the states with positive E_0 are difficult to populate at finite temperature due to the exponential suppression of the Boltzmann factor.

The parabolic form of this curve can be explained by the observation that with the volume held constant, configurations with predominantly short (or long) bonds cannot distort as effectively as configurations with roughly equal numbers of short and long bonds. For even-valued system size L , this curve should be symmetric about $E_0 = 0$ since there is a relationship between spin states with alternate spins flipped: long bonds become short bonds and vice versa, resulting in a state with E_0 of equal magnitude but opposite sign that has an identical energy shift.

The lack of exact symmetry about $E_0 = 0$ is due to small nonlinearities resulting from non-zero $\bar{\delta}$. Figure 4 shows data for the typical value of $\bar{\delta} = 0.1$ along with a sample of data in which $\bar{\delta}$ was set to 0.01. The results are qualitatively similar, though the smaller-distortion curve is more symmetric.

C. Size Dependence

To study the size dependence of the energy, data for ΔE and σ was collected for system sizes from $L = 3$ to 40. For all system sizes, the shift in the average energy displays the parabolic shape shown in Figs. 3 and 4, and the similarity in form suggests that the curves may be made to collapse. Fig. 5(a) contains the results for $\Delta E / \mu$ for the full range of system sizes simulated. 100

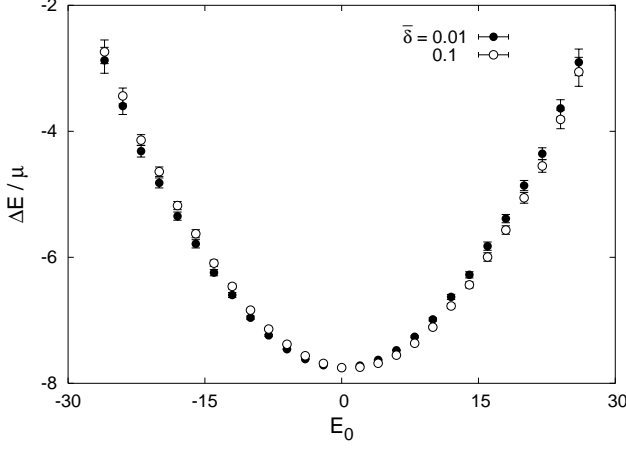


FIG. 4: The effect of changing the distortion parameter $\bar{\delta}$, as defined in Eq. (2), is shown for the fully enumerated systems with $L = 4$ and $\mu = 0.1$. The parabolic form of the data is unchanged; however, the smaller value of the typical distortion size results in a curve that is slightly more symmetric about $E_0 = 0$. 100 systems were averaged to produce these data.

systems were averaged at each system size; in the figure, data points are only displayed for values of E_0 where at least 20 systems were represented. The $L = 3, 4$, and 5 systems were fully enumerated, while the larger systems were run at a series of temperatures to obtain data over a range of values of E_0 . As the inset in that figure demonstrates, when both axes are scaled by L^2 , the data for the various system sizes approach a constant curve as L increases. While there are finite-size effects in the smallest systems, the data for $L \geq 10$ collapse quite well.

The quadratic form of the scaled data for ΔE is expressed as

$$\frac{\Delta E}{\mu L^2} = A_{\Delta E} \times \left(\frac{E_0}{L^2} - B_{\Delta E} \right)^2 + C_{\Delta E}. \quad (4)$$

The locations of the minima for each system size were averaged to determine the global horizontal offset: $B_{\Delta E} = 0.063 \pm 0.001$. With $B_{\Delta E}$ determined, the $L = 40$ data were then fit to the parabolic form above, with $A_{\Delta E} = 0.1166 \pm 0.0007$ and $C_{\Delta E} = -0.5004 \pm 0.0008$. The main panel of Fig. 5(a) shows the data and fit plotted in a manner that makes the collapse to the form of Eq. (4) apparent.

Data for the width of each band also demonstrate a quadratic function of E_0 , as shown in Fig. 5(b). As with the energy shift, the σ data for the various system sizes can be scaled to lie on a common curve; however, while the E_0 axis is again scaled by the system size L^2 , the width axis is only scaled by the linear size of the system, L .

The scaled data for the width are described by the form

$$\frac{\sigma}{\mu L} = A_{\sigma} \times \left(\frac{E_0}{L^2} - B_{\sigma} \right)^2 + C_{\sigma}. \quad (5)$$

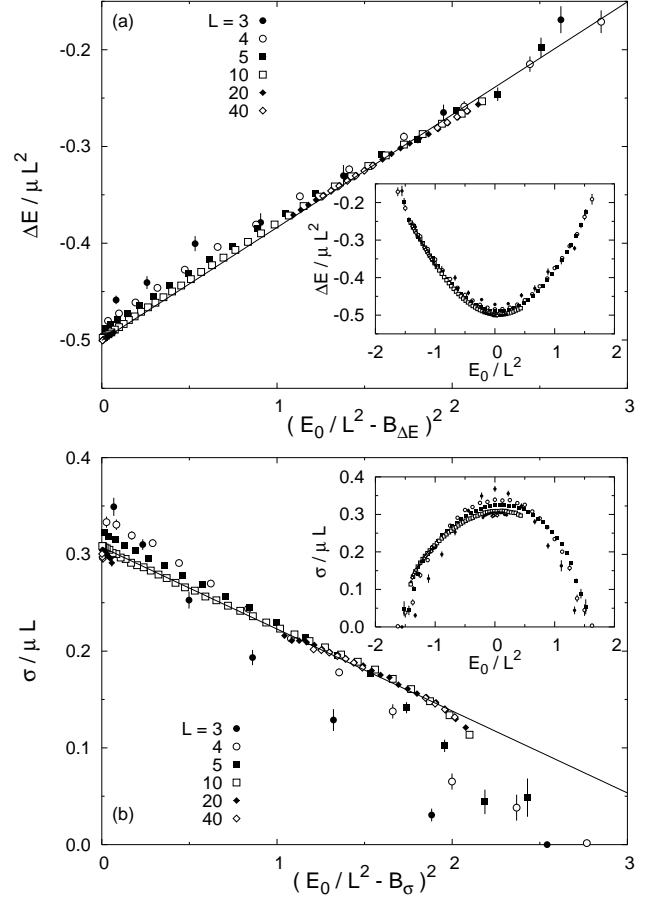


FIG. 5: System-size scaling. (a) The slope of the average energy shift, as a function of E_0 , with both axes scaled by L^2 . As L increases, the data for different system sizes collapse onto a common curve that is quadratic in E_0 . The main panel shows the data plotted and fit according to the form of Eq. (4), while the inset shows the scaled data directly. (b) The data for the spread in energy as a function of E_0 can also be made to approach a common parabolic curve; however, while the E_0 -axis is again scaled by L^2 , the width axis is scaled by the linear size only.

As with ΔE , data from all sizes were used to obtain $B_{\sigma} = 0.039 \pm 0.004$. The $L = 40$ data were then fit to Eq. (5), resulting in $A_{\sigma} = -0.085 \pm 0.002$ and $C_{\sigma} = 0.308 \pm 0.003$. Figure 5(b) shows the data and fit line.

The scaling behavior of σ implies an interesting side effect of the introduction of compressibility. Since E_0 is proportional to L^2 , the total number of spins, the right-hand side of Eq. (5) is independent of L , and thus $\sigma \sim \mu L$. Neighboring energy bands will overlap to a large degree when the width of the bands is comparable to the spacing between them, i.e., when $\mu L \sim 4$. As $L \rightarrow \infty$, an infinitesimal value of the coupling will satisfy this condition, rendering the previously discrete energy spectrum continuous.

While the forms of ΔE and σ are similar, it is not immediately apparent that the two quantities are directly

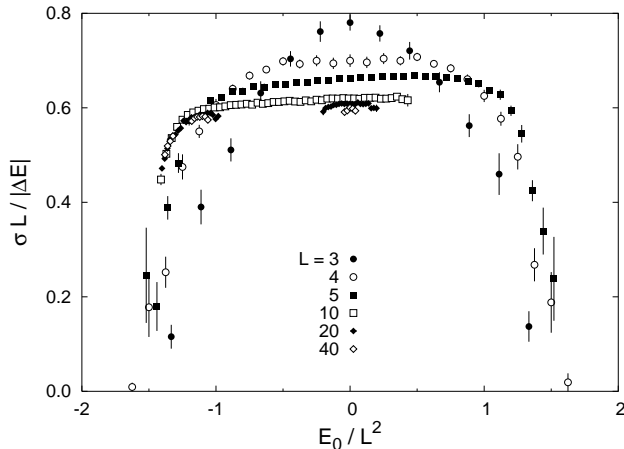


FIG. 6: The ratio of the width to the magnitude of the energy shift as a function of E_0 for different system sizes; the axes have been scaled by L and L^2 , respectively, to demonstrate an approach to constant behavior as the system size increases. Plotted this way, the scaled ratio is less than a constant of order unity. Thus, σ becomes negligible compared to ΔE for large L .

related. In fact, over a large range of E_0 , the spread in energy is proportional to the energy shift, as shown in Fig. 6, where the data displayed in Fig. 5 are plotted as a ratio of $\sigma \times L$ to the absolute value of ΔE versus E_0 / L^2 . Again, the data from different system sizes were made to collapse by appropriate scaling of the axes.

It is apparent from Fig. 6 that the magnitude of the scaled ratio is less than a constant, ρ , with $\rho \approx 0.6$ for large values of L . The relationship between σ and ΔE can be expressed as

$$\sigma \lesssim \frac{\rho}{L} |\Delta E|. \quad (6)$$

Thus, as the system size increases, the width of a band of states becomes negligible compared to the magnitude of the shift in energy from its uncoupled value.

V. SIMPLIFIED MODEL

The form of ΔE , as demonstrated in Figs. 3, 4, and 5(a) and expressed by Eq. (4), is a quadratic function of E_0 . In addition, the spread in the energy becomes negligible compared to the energy shift for large system sizes, as Eq. (6) demonstrates. These observations motivate²⁵ an approximate Hamiltonian for the compressible spin glass:

$$\mathcal{H}_{\text{approx}} = - \sum_{\langle i,j \rangle} J_{ij} S_i S_j + \frac{\nu}{L^2} \left(\sum_{\langle i,j \rangle} J_{ij} S_i S_j \right)^2. \quad (7)$$

The sum that appears in both terms is performed as described for the original Hamiltonian of Eq. (1), and numerical factors—such as $A_{\Delta E}$ from Eq. (4)—have been

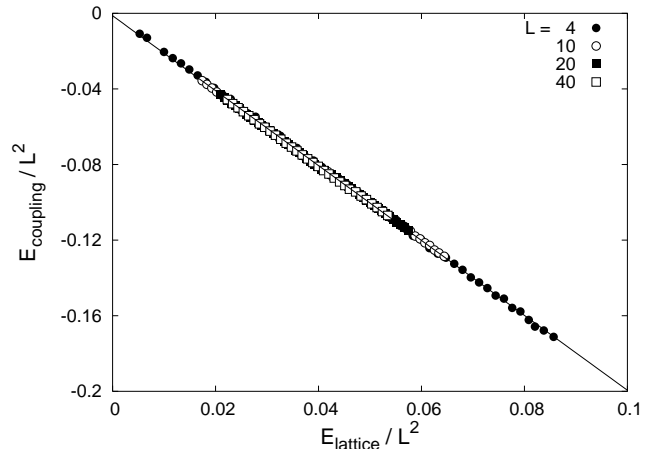


FIG. 7: A selection of data from various system sizes shows the relationship between the two position-dependent components of the total energy given by Eq. (1); here, the second term (representing the energy due to the coupling, E_{coupling}) is plotted versus the third term (the lattice energy, E_{lattice}) for individual spin configurations. Both axes are scaled by L^2 to bring the data from different system sizes into a common range. As the coupling energy is proportional to the lattice energy, these two terms may be combined into a single term that describes the energy shift due to particle motions in the presence of the coupling.

absorbed into the coupling constant so that $\nu \approx 0.12\mu$. Again, the first term represents the energy due to spin-spin interactions, denoted E_0 . The second term, which contains the coupling between the spins and the lattice, can be viewed as a combination of the final two terms of Eq. (1) with a typical distortion of the order of $\bar{\delta}$ as defined in Eq. (2).

That the two position-dependent components of the total energy may be combined in this way is shown explicitly in Fig. 7, where the coupling energy is plotted against the lattice energy for data obtained in the previously described simulations. Both axes are scaled by L^2 to bring the points from different system sizes into a common range, and the solid line is a linear fit to all of the data. The coupling energy is proportional to the lattice energy, and since the two terms are related in a straightforward manner, their net effect may be represented by a single term in the simplified Hamiltonian.

I note some features of the approximate model. First, the system size must be included explicitly in order to preserve the observed scaling behavior. Second, rather than being constructed from a combination of parameters, the coupling constant ν is directly present and controls the strength of the compressibility term. Finally, and most importantly, this Hamiltonian contains only spin degrees of freedom; the positional variables are absent, and the degrees of freedom associated with them have been absorbed into the second term of Eq. (7). Thus, the simplified model can be viewed as a mean-field version of the original Hamiltonian, where the energy due

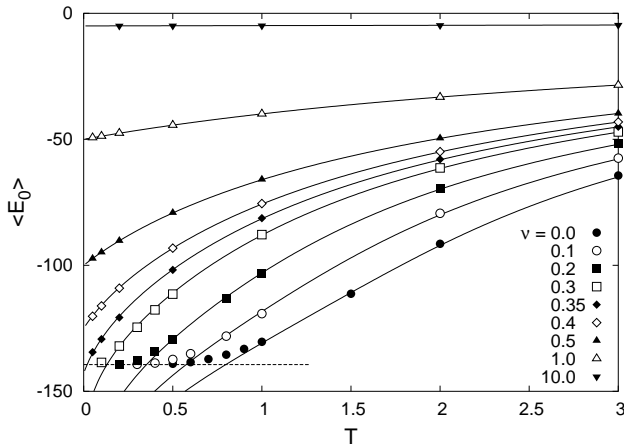


FIG. 8: Results from Monte Carlo simulations of the approximate model of Eq. (7) on 100 systems with $L = 10$. The average value of E_0 is plotted as a function of T for various values of ν . Below a critical value, $\nu^* \approx 0.35$, the energy approaches that of the ground state (dashed line) as $T \rightarrow 0$; above ν^* , the energy limit is predicted by Eq. (10). The solid lines are not fits; rather, they represent predictions obtained by minimizing the free energy using the entropy form of Eq. (14). This figure is reprinted from Ref. 25.

to local distortions has been replaced by an energy contribution that is typical for states with equivalent spin energy. As a practical matter, this feature also means that simulations and analytical work may be performed on the model using techniques identical to those used in standard (incompressible) spin-glass studies.

A. Simulation Results

To simulate the model described in the simplified Hamiltonian, single-spinflip Monte Carlo simulations were performed at various values of the coupling as parametrized by ν . As in standard Monte Carlo spin-glass simulations, for each bond realization a sequence of spin states was generated at a fixed temperature T , with transition probabilities between states based on the difference in energy as calculated from Eq. (7).

To monitor which states of the compressible spin glass are favored at a given value of T and ν , the thermal- and disorder-averaged values of E_0 , denoted $\langle E_0 \rangle$, are calculated. Results for 100 systems with $L = 10$ are shown as data points in Fig. 8. Solid lines in that figure represent predictions based on the free-energy analysis described below in Sec. V C.

For each value of ν , the average value of E_0 decreases as the temperature is lowered (at infinite temperature, $\langle E_0 \rangle = 0$ since the $E_0 = 0$ states have the highest entropy). For small values of ν , as $T \rightarrow 0$, the data approach the ground-state energy of the uncoupled system, indicated by the dashed horizontal line in the figure. For each curve as a function of T , the inflection point

represents the temperature at which the presence of the ground states of the uncoupled system becomes important. Below this temperature, those ground states begin to be populated, halting the decrease in $\langle E_0 \rangle$. As the coupling is increased, the inflection point moves down in temperature, eventually disappearing when $\nu \approx 0.35$. For larger values of the coupling, there is no inflection point, and the data for $\langle E_0 \rangle$ no longer approach the ground-state energy as $T \rightarrow 0$ but rather terminate at some higher value that increases with increasing ν .

The heat capacity can be calculated as the fluctuations in the energy about its average value, divided by the square of the temperature. For the simplified model of the compressible spin glass, the specific heat shows no interesting features, going smoothly to zero as $T \rightarrow 0$. However, a similar quantity, using E_0 instead of the total energy, can be calculated:

$$\hat{C} \equiv \frac{\langle E_0^2 \rangle - \langle E_0 \rangle^2}{T^2}. \quad (8)$$

Data for \hat{C} from the simulations of the simplified model are shown as points in Fig. 9(a). Solid lines in that figure are predictions based on the free-energy analysis described below.

At small values of ν , the data and corresponding prediction for \hat{C} are peaked. For $\nu = 0$, i.e., the standard Ising spin glass, this peak is interpreted as signaling the onset of critical behavior that precedes the spin-glass transition as the temperature continues to be lowered.³ As the coupling approaches a critical value, ν^* , the temperature at which the peak in \hat{C} is located moves toward zero, and the height of the peak, \hat{C}_{\max} , diverges. Figure 9(b) shows that this divergence is a power law:

$$\hat{C}_{\max} = A(\nu^* - \nu)^{-p}.$$

The points in that figure are the locations of the maxima, as obtained from parabolic fits to data near the peak of each curve as a function of T , while the solid line is a power-law fit to the peaks of the predicted curves with $\nu^* = 0.365$ and a power-law exponent of 1.3. The reasons for the divergence are discussed below.

B. Analytic Results

For the approximate Hamiltonian of Eq. (7), there is a one-to-one correspondence between the spin energy E_0 (calculated as before) and the total energy. To understand the results of the simulation as presented in Fig. 8, it is useful to analyze the expected value of the energy for various values of the control parameters. In simplified notation, Eq. (7) can be written²⁵

$$E = E_0 + \frac{\nu}{L^2} E_0^2. \quad (9)$$

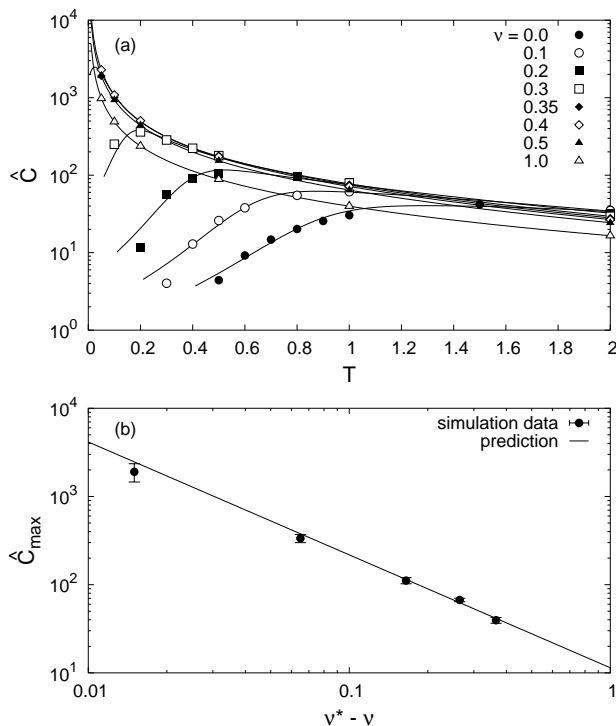


FIG. 9: (a) The heat-capacity-like quantity \hat{C} —defined in Eq. (8)—as a function of T for different values of ν , calculated from simulations of the simplified model on 100 averaged systems with $L = 10$. The peak in \hat{C} shifts downward in T as ν increases. The solid lines are predictions based on the free-energy analysis described in Sec. V C. (b) The maximum value of \hat{C} demonstrates a power-law divergence as ν approaches a critical value, ν^* . The points are obtained from polynomial interpolation of data near the peak of each curve in panel (a). The solid line is a fit to the peaks of the \hat{C} prediction curves as a function of ν ; from the fit, $\nu^* = 0.365$, and the power-law exponent is 1.3.

Taking the derivative with respect to E_0 allows one to calculate the value of the spin energy, $E_{0,\min}$, that minimizes the total energy as function of ν :

$$E_{0,\min} = \frac{-L^2}{2\nu}. \quad (10)$$

This represents the expected value of the spin energy as $T \rightarrow 0$; however, the calculated value is not necessarily realizable, since E_0 must be greater than the ground-state spin energy $E_{0,\text{gnd}}$. For small values of ν , the calculated value of $E_{0,\min}$ lies in the non-physical region below $E_{0,\text{gnd}}$, and thus the minimum spin energy is, of course, equal to the ground-state spin energy. This explains the form of the small- ν data in Fig. 8, where the average spin energy decreases with temperature but approaches $E_{0,\text{gnd}}$ asymptotically as $T \rightarrow 0$.

There is a value of ν at which the minimum E_0 becomes equal to the ground-state energy of the uncoupled

system, $E_{0,\text{gnd}}$:

$$\nu^* \equiv \frac{-L^2}{2E_{0,\text{gnd}}}. \quad (11)$$

For the two-dimensional spin-glass, the ground-state energy per spin is -1.4 ,⁸ and thus $\nu^* = 0.36$. This value is the same as the value of ν at which the simulation data, as shown in Figs. 8 and 9, display a change in behavior.

At $\nu = \nu^*$, the nature of the energy spectrum is dramatically altered: As the coupling increases from zero, higher- E_0 states shift downward in energy more rapidly than lower- E_0 states, and thus the difference in total energy between neighboring E_0 levels becomes smaller. The value ν^* represents the coupling at which the ground state and first excited state of the uncoupled system have the same total energy. Above this value, states with $E_0 = E_{0,\text{gnd}}$ no longer have the lowest total energy, and as ν increases still more, increasingly higher E_0 -levels are associated with the ground states of the compressible system. The data in Fig. 8 display this feature, as the zero-temperature value of $\langle E_0 \rangle$ increases with the coupling for $\nu > \nu^*$. The divergence in \hat{C} , as shown in Fig. 9, is also a consequence of this change in the energy spectrum. As $\nu \rightarrow \nu^*$, the difference in total energy between levels near $\langle E_0 \rangle$ goes to zero, and thus the fluctuations in E_0 no longer vanish as $T \rightarrow 0$.

C. Free Energy Analysis

In order to predict which states are preferred as a function of ν and T , the free energy must be minimized, and for this a functional form for the entropy is needed. The probability of generating a state of given energy is proportional to the Boltzmann-weighted density of states: $P(E) \propto \Omega(E) \exp(-E/T)$; from this the entropy $S(E)$ is derived as $\log \Omega$. Since the density of states is a function of the uncoupled energy, i.e., $\Omega = \Omega(E(E_0))$, it may be calculated for any value of the coupling. For a given ν and T , simulations will produce a limited range of energies that will be populated with statistical significance; data is therefore acquired at different couplings and temperatures to produce overlapping regions of data that may be combined. Since for each run the proportionality between the generated probabilities and the density of states is unknown, it is more convenient to generate the derivative of the entropy:

$$\frac{dS}{dE_0} = \frac{d}{dE_0} [\log P(E_0) + E(E_0)/T]. \quad (12)$$

Data for the derivative of the entropy is shown in Fig. 10. For each system size, 100 individual bond configurations were run at a variety of temperatures and averaged. By plotting dS/dE_0 versus E_0 per spin, the data from different system sizes are made to lie on a single curve. This curve is linear over a large region passing

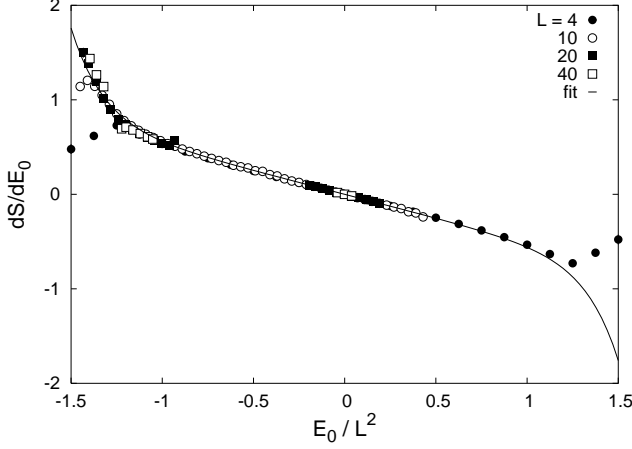


FIG. 10: Data for the derivative of the entropy, averaged over 100 systems each at sizes from $L = 4$ to 40. When plotted as a function of E_0 per spin, the data lie on a common curve that is well fit by the functional form given in Eq. (13).

through $E_0 = 0$, and the deviations from linearity are exponential. As demonstrated by the solid line in Fig. 10, the overall curve is well fit by the functional form

$$\frac{dS}{dE_0} = -c_1 \frac{E_0}{L^2} - c_2 \sinh\left(c_3 \frac{E_0}{L^2}\right), \quad (13)$$

where $c_1 = 0.5$, $c_2 = 4.5 \times 10^{-4}$, and $c_3 = 5.6$. The entropy is thus of the form

$$S(E_0) = S_0 - S_1 E_0^2 - S_2 \cosh(S_3 E_0), \quad (14)$$

with $S_1 = 0.25/L^2$, $S_2 = 8.1 \times 10^{-5} L^2$, and $S_3 = 5.6/L^2$.

With the entropy given by Eq. (14) and the energy given by Eq. (9), the free energy, $F = E(E_0) - TS(E_0)$, may be minimized with respect to E_0 . The spin energy of the system in the thermodynamic limit is thus given by the solution to the equation

$$1 + \frac{2\nu}{L^2} E_0 + 2TS_1 E_0 + TS_2 S_3 \sinh(S_3 E_0) = 0.$$

While this equation cannot be solved analytically, it is possible to obtain a numerical solution as a function of ν and T . Such results are plotted as solid lines in Fig. 8, where the values of $\langle E_0 \rangle$ as predicted from the free-energy calculation are in excellent agreement with those obtained from simulations of the simplified model. The predictions tend to diverge from the data at low temperatures for small values of the coupling; this is the regime in which the lowest-energy states are heavily populated and the functional form for the entropy—which contains no low-energy cutoff—ceases to be a good description of any actual system.

The free energy described above was also used to predict values for the heat-capacity-like quantity \hat{C} , as defined in Eq. (8). These predictions are shown for various values of the coupling as the solid lines in Fig. 9(a); the

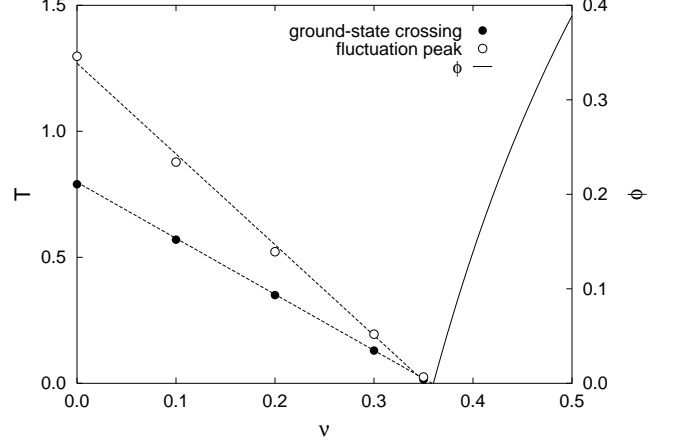


FIG. 11: Phase diagram in the $\nu - T$ plane showing the temperature at which the predicted energy crosses the ground-state energy and the temperature at which the peak in \hat{C} occurs. Dashed lines indicate linear fits to these data; the two lines terminate at ν^* . The region beneath the lines represents the critical regime, signaling the onset of the spin-glass phase. At the same value ν^* , the order parameter ϕ —defined in Eq. (15)—increases linearly from zero, indicating the suppression of critical behavior.

agreement with data from the simulations is very good except at low temperatures for small ν , where the applicability of this form for free energy is expected to break down. Near the peaks in \hat{C} , however, the predictions are still in reasonable agreement with the simulation results. The peaks of the predicted curves were thus used to generate a prediction for the divergence of \hat{C}_{\max} . The power-law fit to these peaks is shown as the solid line in Fig. 9(b), where the power-law exponent is 1.3 and $\nu^* = 0.365$, consistent with the value of 0.36 obtained via Eq. (11).

D. Phase Diagram

It is possible to map out various quantities as a function of ν and T . Consider the temperature at which the predicted value of $\langle E_0 \rangle$ crosses the ground-state energy of the uncoupled system (see Fig. 8). This represents the breakdown of the prediction due to the lack of a consistent analytic form for the entropy near the ground state. Near this temperature, there is an inflection point in the curve of the average E_0 as the presence of the ground state becomes important and the curve begins to flatten. Also of interest is the location of the peak in \hat{C} with respect to T , which indicates the onset of critical spin-glass behavior. Both of these quantities, calculated from the predictions described in Sec. V C, are plotted in a $\nu - T$ phase diagram in Fig. 11, with linear fits to the points.

The lines in the $\nu - T$ plane mark an approximate phase boundary between the normal (paramagnetic) phase and the critical regime that signals the onset of spin-glass be-

havior. The fit lines for the ground-state crossing and the peak in \tilde{C} terminate at $\nu = 0.359$ and 0.353 , respectively, consistent with the value of ν^* predicted from Eq. (11). Commensurate with the termination of these lines at ν^* is the growth from zero of an order parameter characterized by the difference between the minimum value of E_0 and the ground-state energy of the uncoupled system:

$$\phi = E_{0,\min} - E_{0,\text{gnd}}. \quad (15)$$

Using Eqs. (10) and (11), it is apparent that ϕ grows as $1/\nu^* - 1/\nu$, i.e., linear just above the critical value ν^* . Figure 11 shows this phenomenon.

The interpretation of ϕ is as a measure of the inaccessibility of low- E_0 states, even at low temperatures, due to the presence of the coupling to lattice distortions. These states, at and near the ground state of the uncoupled system, are no longer the lowest-energy states of the compressible spin glass, and the competition between energy and entropy no longer exists. Non-zero ϕ is thus correlated with the suppression of critical behavior that precedes the spin-glass phase; above ν^* , the spin-glass transition cannot exist.

VI. CONCLUSIONS

This paper has analyzed a model²⁵ for a compressible Ising spin glass that lends itself to simulations similar to those for standard spin glasses, with additional steps to determine the positions of the spin particles. While exploration of the dynamics of this system has proven difficult, it is possible to characterize the effect of the coupling to lattice distortions on the energy of the system. Both the shift in energy and the width of each band of states display parabolic shapes as a function of the uncoupled energy E_0 , and system-size scaling demonstrates that the width becomes negligible compared to the energy shift as L increases.

The form of the shift in energy due to the presence of compressibility motivates a simplified model for the compressible spin glass.²⁵ This model, which depends only upon spin degrees of freedom, was simulated using standard techniques. In addition, analysis of the simplified model suggests a critical value of the coupling above which the nature of the energy levels changes dramatically, and the simulation data confirm this. Due to the

elimination of the critical regime, a spin-glass transition cannot exist above this critical value.

The simplified model adds long-range interactions to the nearest-neighbor behavior of the standard Edwards-Anderson model for the spin glass. This provides a convenient mechanism for incorporating phonon effects into theoretical spin-glass studies, and it is possible that consideration of these effects may help to shed light on some experimental results that have yet to be fully explained. For example, work by Bitko et al.²⁴ demonstrated the existence of a signature for the spin-glass transition at high frequencies, hinting that coupling to high-frequency modes (such as phonons) may be important.

I expect the results not to change qualitatively in three dimensions. Preliminary studies similar to those described above suggest that, as for the two-dimensional case, the shift in energy is proportional to the coupling, μ , and to E_0 ². Furthermore, the energy shift scales as the volume of the system, L^3 , while the spread in each energy band scales as L . Thus, the assumptions that led to the simplified model of Eq. (7) hold even more strongly in three dimensions; similar results for the elimination of the spin-glass transition above a critical value of the coupling should then follow, but additional work is required to verify this.

It is important to note that many of these results are expected to be quite different if the constraint of constant volume is removed. The quadratic nature of the energy shift (as shown in Figs. 3, 4, and 5) depends on the fact that states at large negative (positive) E_0 cannot distort effectively due to having large numbers of satisfied (unsatisfied) bonds that tend to have similar lengths. A system capable of uniform compression or expansion could take advantage of these states with extreme values of E_0 in an entirely different manner than a system where the volume is constant.

Acknowledgments

I would like to thank S. Nagel and B. Chakraborty for professional guidance and S. Coppersmith, G. Grest, S. Jensen, J. Landry, N. Mueggenburg, and T. Witten for helpful discussions. This work was supported by NSF DMR-0352777 and MRSEC DMR-0213745.

¹ R. N. Bhatt and A. P. Young, Phys. Rev. Lett. **54**, 924 (1985).

² A. T. Ogielski and I. Morgenstern, Phys. Rev. Lett. **54**, 928 (1985).

³ A. T. Ogielski, Phys. Rev. B **32**, 7384 (1985).

⁴ K. Binder and A. P. Young, Rev. Mod. Phys. **58**, 801 (1986).

⁵ R. N. Bhatt and A. P. Young, Phys. Rev. B **37**, 5606

(1988).

⁶ K. H. Fischer and J. A. Hertz, *Spin Glasses* (Cambridge University Press, 1993).

⁷ N. Kawashima and A. P. Young, Phys. Rev. B **53**, R484 (1996).

⁸ J.-S. Wang and R. H. Swendsen, Phys. Rev. B **38**, 4840 (1988).

⁹ L. Saul and M. Kardar, Phys. Rev. E **48**, R3221 (1993).

- ¹⁰ H. Kitatani and A. Sinada, J. Phys. A **33**, 3545 (2000).
- ¹¹ J. Houdayer, Eur. Phys. J. B **22**, 479 (2001).
- ¹² H. G. Katzgraber and L. W. Lee, Phys. Rev. B **71**, 134404 (2005).
- ¹³ C. Amoruso, E. Marinari, O. C. Martin, and A. Pagnani, Phys. Rev. Lett. **91**, 087201 (2003).
- ¹⁴ C. P. Bean and D. S. Rodbell, Phys. Rev. **126**, 104 (1962).
- ¹⁵ D. J. Bergman and B. I. Halperin, Phys. Rev. B **13**, 2145 (1976).
- ¹⁶ Z.-Y. Chen and M. Kardar, J. Phys. C **19**, 6825 (1986).
- ¹⁷ L. Gu, B. Chakraborty, P. L. Garrido, M. Phani, and J. L. Lebowitz, Phys. Rev. B **53**, 11985 (1996).
- ¹⁸ A. Dhar, P. Chaudhuri, and C. Dasgupta, Phys. Rev. B **61**, 6227 (2000).
- ¹⁹ F. Becca, F. Mila, and D. Poilblanc, Phys. Rev. Lett. **91**, 067202 (2003).
- ²⁰ A. B. Sushkov, O. Tchernyshyov, I. W. Ratcliff, S.-W. Cheong, and H. D. Drew, Phys. Rev. Lett. **94**, 137202 (2005).
- ²¹ M. B. Salamon and M. Jaime, Rev. Mod. Phys. **73**, 583 (2001).
- ²² R. Laiho, E. Lähderanta, J. Salminen, K. G. Lisnuov, and V. S. Zakhvalinskii, Phys. Rev. B **63**, 094405 (2001).
- ²³ C. P. Adams, J. W. Lynn, V. N. Smolyaninova, A. Biswas, R. L. Greene, I. W. Ratcliff, S.-W. Cheong, Y. M. Mukovskii, and D. A. Shulyatev, Phys. Rev. B **70**, 134414 (2004).
- ²⁴ D. Bitko, N. Menon, S. R. Nagel, T. F. Rosenbaum, and G. Aeppli, Europhys. Lett. **33**, 489 (1996).
- ²⁵ A. H. Marshall, B. Chakraborty, and S. R. Nagel, Europhys. Lett. **74**, 699 (2006).
- ²⁶ S. F. Edwards and P. W. Anderson, J. Phys. F **5**, 965 (1975).
- ²⁷ W. H. Press, S. A. Teukolsky, W. T. Vetterling, and B. P. Flannery, *Numerical Recipes in C* (Cambridge University Press, 1997), 2nd ed.